International Journal of Heat and Mass Transfer 52 (2009) 4907–4918

Contents lists available at ScienceDirect

International Journal of Heat and Mass Transfer

journal homepage: www.elsevier.com/locate/ijhmt

Experimental investigations of the coupled conductive and radiative heat transfer in metallic/ceramic foams

R. Coquard [a,*], D. Rochais [b,1], D. Baillis [c,2]

[a] Société "Etude Conseils Calcul en Mécanique des Structures" (EC²MS), 66, boulevard Niels Bohr, 69603 Villeurbanne Cedex, France
[b] Commissariat à l'Energie Atomique (CEA)/Le Ripault, BP 16, 37 260 Monts, France
[c] Centre Thermique de Lyon (CETHIL), UMR CNRS 5008, Domaine Scientifique de la Doua, INSA de Lyon, Bâtiment Sadi Carnot, 9 rue de la physique, 69621 Villeurbanne Cedex, France

ARTICLE INFO

Article history:
Received 2 September 2008
Received in revised form 20 April 2009
Accepted 6 May 2009
Available online 7 July 2009

Keywords:
Solid foams
Heat conduction
Thermal radiation
Equivalent thermal conductivity
Laser-FLASH measurement

ABSTRACT

Due to their interesting thermal, mechanical and exchange properties, solid metal or ceramic foams have shown a strong development in numerous technological fields for which the knowledge of their thermal properties is of primary importance. In order to investigate the coupled conductive/radiative heat transfer in this kind of materials, we propose an identification method using thermograms obtained from laser-FLASH measurements. This permits us to evaluate, at ambient and high temperatures, the effective thermal conductivity and two global radiative properties of various metal or ceramic foams, describing the thermal behavior of their equivalent homogeneous semi-transparent materials. This new method of characterization of solid foams is promising since conduction and radiation contributions to heat transfer can be evaluated from a unique experiment.

1. Introduction

During the last decades, the development of solid metal or ceramic foams has permitted the improvement of the performances of standard materials in numerous technological fields. As a matter of fact, they are particularly interesting for applications requiring multifunctionality. They are notably used in ultra light panels, energy absorbing structures, heat dissipation media, electrodes for electric battery, ultrasound deflectors, carrying structures for catalyst, heat exchanger, etc. In most of these applications, a good evaluation of their mechanical, exchange or thermal properties is required to improve the efficiencies of the systems. However, as solid foams are constituted of two different phases, these properties can generally not be evaluated simply. They are related to the properties of the constituents and to the complex morphology of the porous structure. It is particularly true for the thermal properties. Indeed, whilst convective heat transfer could generally be neglected due to the small dimensions of pore sizes, in many applications, the temperatures reached are relatively important and the contribution of radiation heat transfer is significant. Therefore, the thermal behavior is related to the conductive heat transfer but also to the propagation of thermal radiation in the porous structure, which is greatly dependent on the microstructure of the solid matrix.

As regards the conductive heat transfer alone, a great number of theoretical studies have already been conducted on several types of foam. Some of these studies were based on analytical approaches which considered simplified 3porous structures. We can cite the work of Schuetz and Glicksmann [1,2], Boomsma and Poulikakos [3], or Battacharya et al. [4]. More sophisticated numerical methods were also developed notably by Druma et al. [5], Saadatfar et al. [6] or, very recently, by Coquard et al. [7]. Some of these models were applied to theoretical representations of the cellular morphology [5,7], permitting to investigate the influence of the structural parameters. The methods developed were also applied to 3-D representations of the microstructures obtained from X-ray tomography [6]. Most of the analytical and numerical models were validated by thermal conductivity measurements on solid foams at ambient temperature. All these studies show that the magnitude of heat conduction in metal or ceramic foams is closely related to the density and to the morphology of the microstructure but is practically independent of the size of the pores.

At the same time, several experimental or theoretical studies were conducted uniquely on the radiative heat transfer. Petrasch et al. [8] investigated theoretically the radiative heat transfer in reticulated porous ceramics using a Monte Carlo method applied to 3-D tomographic representations of the microstructure. Zeghondy et al. [9] have proposed a radiative distribution function identification (RDFI) to obtain the extinction and absorption coefficients and the bidirectional phase function of porous

* Corresponding author. Tel.: +33 4 37 48 84 09; fax: +33 4 37 48 84 05.
E-mail addresses: remi.coquard@ec2-ms.fr (R. Coquard), denis.rochais@cea.fr (D. Rochais), dominique.baillis@insa-lyon.fr (D. Baillis).
[1] Tel.: +33 2 47 34 42 82.
[2] Tel.: +33 4 72 43 84 74.

0017-9310/$ - see front matter © 2009 Elsevier Ltd. All rights reserved.
doi:10.1016/j.ijheatmasstransfer.2009.05.015

Nomenclature

C	specific heat of the foam sample (J/kg/K)
C_{coat}	specific heat of the interface coating (J/kg/K)
D_{cell}	cell diameter (m)
e	thickness of the black coating (m)
$\vec{e}_r, \vec{e}_z$	unit vector of the radial and axial axis
h	convective heat transfer coefficient (W/m^2/K)
$I^{\lambda}_{r,z,\vec{\Delta}}$	spectral radiant intensity at the point of coordinates (r, z) in the direction $\vec{\Delta}$ (W/m^2)
$I^{m}_{i,j}$	radiant intensity at the discrete point (i, j) in the discrete direction m (W/m^2)
$I^{\lambda}_0(T)$	spectral radiant intensity of the black body at temperature T (W/m^2)
k_c	effective thermal conductivity of the foam sample (W/m/K)
k_{coat}	thermal conductivity of the interface coating (W/m/K)
L	width of the foam sample (m)
nR	number of spatial discretization along the radial axis
nZ	number of spatial discretization of the sample along the axial axis
nZ_{coat}	number of spatial discretization of the interface coating along the axial axis
$P_\lambda(v)$	spectral scattering phase function
$\vec{q}$	heat flux density (W/m^2)
Q	FLASH heating power per surface unit (W/m^2)
r	radial coordinate
$R_{\max}$	radius of the sample (m)
S_λ	spectral specularity parameter
t	time (s)
t^*	dimensionless time = $t/\Delta t$
T	temperature (K)
T_{coat}	temperature of the interface coating (K)
T_{ext}	external temperature (K)
T_s	temperature of the external surfaces of the sample (K)
w_m	weighting factor for the mth direction of the angular discretization
z	axial coordinate

Greek symbols

β_λ, σ_λ and κ_λ	spectral extinction, scattering and absorption coefficients (m^{-1})
β^*	scaled extinction coefficient identified
$\omega_\lambda = \sigma_\lambda/\beta_\lambda$,	spectral scattering albedo
ω^*	scaled scattering albedo identified
$\varepsilon^{\lambda}_{coat}$	spectral emissivity of the interface coating
ϕ	radial angle
ρ	density of the foam (kg/m^3)
ρ_{air}	density of air (kg/m^3)
ρ_{coat}	density of the interface coating (kg/m^3)
ρ_{solid}	density of the bulk solid phase (kg/m^3)
λ	radiation wavelength (μm)
Ω	solid angle
σ_{SB}	Stefan-Boltzmann constant ($\approx 5.67 \times 10^{-8}$ W/m^2/K^4)
(μ_m, η_m, ξ_m)	directing cosine of the discrete directions of the quadrature
$\langle\mu\rangle_\lambda = \int_0^\pi P_\lambda(\theta)\cdot\cos\theta\cdot\sin\theta\cdot d\theta$	asymmetry parameter
τ	duration of the pulse irradiation (s)
Δt	measurement duration (s)
Δr_i	dimension of the dicretised volume along the radial axis (m)
Δz_j	dimension of the dicretised volume along the axial axis (m)

Subscripts

c	conductive
exp.	experimental
num.	numerical
r	radiative
t	total
i, j	at the point of coordinates (r_i, z_j)
th.	theoretical
ident.	identified

Superscripts

z	along the axial axis
r	along the radial axis
l	at the lth iteration
m	mth direction of the quadrature
0	initial
t	at tth iteration time

materials. Their method only requires the knowledge of the material morphology, given by a X-ray tomography and the local radiative properties of the phases. They applied their method to mullite foams [10]. Loretz et al. [11] conducted a review of the analytical models of computation of the radiative properties of solid foams taking into account a wide variety of cells shape and struts cross sections. These theoretical results were compared to radiative properties of different high-porosity metal foams identified from spectrometric measurements. Thus, the authors have determined the models and microstructure representations that best simulate the radiative behavior of this type of foams. Zhao et al. [12] studied experimentally the radiative behavior of FeCrAlY foams by conducting transmittance and reflectance measurements. They show that the radiative behavior, which varies significantly with the wavelength considered, is mostly influenced by the cell size and the density of the foams. The development of an analytical model based on empirical formulas permit them to predict accurately the variations of the radiative behavior of the foams with the wavelength and with the structural parameters. Zhao et al. [13] also developed an analytical explicit model characterizing the radiative transport process in highly porous, open-celled metal foams having idealized cellular morphologies. They show that the equivalent radiative conductivity increases linearly with increasing cell size, whilst for a given cell size the variation of relative density only has a small effect on radiation.

At last, other researchers have been interested in the modeling of the total heat transfer at high temperatures, taking into account both conductive and radiative contributions. Lu and Chen [14] had recourse to an analytical approach to treat the radiative heat transfer through aluminium foams used as a fire retardant. Wang and Pan [15] developed a random generation-growth method to reproduce numerically the microstructures of open-cell foam and applied the Lattice-Boltzmann method and empirical formulae to treat the conductive and radiative heat transfer, respectively. Experimental investigations on the radiative/conductive heat transfer in solid foams were also conducted notably by Zhao et al. [16] on FeCrAlY foams. The authors made a series of measurements of the equivalent conductivity on several foams under various pressure and temperature conditions, using a guarded hot plate apparatus. They show that the equivalent thermal conductivity increases significantly with temperature. Although their experimental equipment did not allow them to separate radiative and conductive contributions, they attribute this increase to the enhancement of the radiative heat transfer.

We can see that the literature on the modeling of radiative or conductive heat transfer in metal or ceramic foams is abundant, but the number of experimental studies remains relatively limited. Moreover, these experimental investigations generally concern the radiative or the conductive heat transfer alone and require heavy equipments, especially for measurements at high temperatures. As a matter of fact, it is not possible, by now, to evaluate both radiative and conductive parts simultaneously from a unique simple measurement. To remedy this problem, we propose a new approach based on classical FLASH experiments. The method appeals to a direct simulation of the transient combined radiation–conduction heat transfer coupled with an identification procedure. The modeling of FLASH experiments in a conductive and semi-transparent material has already been conducted by several authors. André and Degiovanni [17,18] solved the coupled transient heat transfer problem in a plane-parallel slab of purely absorbing materials submitted to a pulse irradiation. They show that the radiative contribution leads to noticeable errors of the FLASH measurement for this kind of materials. However, under conditions of small optical thicknesses and reflecting walls, the heat transfer in the sample is completely free from any radiative contribution. This permits them to estimate the true thermal conductivity of float glass and silica glass. Hahn et al. [19] have also modeled the transient combined radiative/conductive heat transfer and applied it to the simulation of laser-FLASH measurements on ceramic powder compacts. They assumed isotropic scattering and used the three-flux approximation. Their numerical results show that the classical laser-FLASH measurements may lead to a considerable overestimation of the diffusivity in heterogeneous semi-transparent materials at elevated temperatures due to the radiative contribution. Lazard et al. [20] have developed a semi-empirical model based on the kernel substitution technique which simulates the combined conductive–radiative heat transfer in a plane-parallel slab submitted to a pulse irradiation. This model is used to estimate the phononic conductivity and some radiative parameters from FLASH experiments. They show that their new approach allows an accurate estimation of the phononic conductivity even when the radiative contribution is significant whereas classical FLASH technique overestimates this conductivity. However, the radiative properties estimated by their method are not usable.

By contrast, the method proposed in this study allows theoretically the estimation of both conductive and radiative properties of the equivalent isotropic semi-transparent material. The method requires a direct simulation of the transient combined radiation–conduction heat transfer using the discrete ordinates method and the finite volume method. The principle is to minimize the discrepancy between experimental and theoretical thermograms. The number of properties required to simulate the radiative heat transfer in the foam is relatively high. Consequently, we reduced the number of these parameters to identify. We managed to characterize accurately the thermal behaviors of the foam samples using only three identification parameters: one parameter (the effective thermal conductivity k_c) dedicated to conductive heat transfer and two parameters (scaled extinction coefficients β^* and albedo ω^*) characterizing the radiative heat transfer. First, we describe the coupled transient heat transfer model and the identification procedure used. Thereafter, we explain the choice of the thermal parameters retained for the identification. Despite the simplification of the model, we show theoretically that the thermal behavior of the foam sample is well reproduced by the parameters chosen. Finally, we apply our identification method to experimental thermograms obtained on several metal and ceramic foams. The thermal properties identified and their evolutions with the temperature and with the structural characteristics of the foams are compared to theoretical conclusions of previous studies.

2. Theoretical considerations

Our method of characterization of the thermal behavior of the foams consists in the identification of the isotropic conductive and radiative parameters from the thermograms obtained by a FLASH measurement. The identification procedure is based on a least-square fit method and requires an accurate theoretical modeling of the transient heat transfer in the foam. First, we describe the model developed to simulate the thermal transfer in the sample. Then, we detail the principle of the identification procedure that permits to estimate the radiative and conductive parameters from the experimental thermograms. Finally, we present the radiative and conductive parameters that we retained for the identification method.

2.1. Direct simulation of the FLASH measurement

The principle of FLASH experiments is to generate a pulse heating of the front face of a cylindrical sample. Then, we measure the increase of the temperature at the rear face (see Fig. 1). The pulse heating is obtained by a pulse irradiation and, thus, the faces have to be covered with a black coating of known thermal properties and thickness e. The thermogram measured allows estimating the thermal conductivity of the isotropic material. However, in our study, contrary to the hypothesis generally used for a classical FLASH measurement, the foam samples tested could not be considered as purely conductive materials but rather as semi-transparent materials in which the propagation of thermal radiation is significant. Therefore, the theoretical model should simulate accurately the coupling between conductive and radiative transfer.

2.1.1. Governing equations

The thermal balance in a material submitted to a transient heat transfer is governed by the energy equation relating the variation of the local temperature to the total heat flux divergence. In the interface coating, the heat is only transferred by conduction:

$$\rho C \frac{\partial T_{coat}}{\partial t} = -\nabla(\vec{q}_t) = -\nabla(\vec{q}_c) \tag{1}$$

In the solid metal or ceramic foams, the convective heat transfer could be neglected and the equation reduces to:

$$\begin{aligned}\rho C \frac{\partial T}{\partial t} &= -\nabla(\vec{q}_t) = -[\nabla(\vec{q}_r) + \nabla(\vec{q}_c)] \\ &= k_c \cdot \frac{\partial^2 T}{\partial r^2} + \frac{1}{r} \cdot k_c \cdot \frac{\partial T}{\partial r} + k_c \cdot \frac{\partial^2 T}{\partial z^2} - \nabla(\vec{q}_r)\end{aligned} \tag{2}$$

The radiative heat flux is related to the spectral intensity fields in the medium:

$$\vec{q}_r = q_r^r \cdot \vec{e}_r + q_r^z \cdot \vec{e}_z \tag{3}$$

$$\text{with} \quad q_r^r(r,z) = \int_{\lambda=0}^{\infty} \int_{\Omega=4\pi} I^{\lambda}_{r,z,\vec{\Delta}} \cdot \mu \cdot d\Omega \cdot d\lambda;$$

$$q_r^z(r,z) = \int_{\lambda=0}^{\infty} \int_{\Omega=4\pi} I^{\lambda}_{r,z,\vec{\Delta}} \cdot \xi \cdot d\Omega \cdot d\lambda \tag{4}$$

$$\text{and} \quad \nabla(\vec{q}_r) = \frac{1}{r} \cdot \frac{\partial}{\partial r}(r \cdot q_r^r) + \frac{\partial q_r^z}{\partial z} \tag{5}$$

The spectral radiation intensity field is governed by the radiative transfer equation (RTE) described in details in [21]. It takes into account the emission, the absorption and the scattering of the radiation by the participating medium. For a 2-D axisymmetric radiative transfer in an isotropic material with azimuthal symmetry, this equation is:

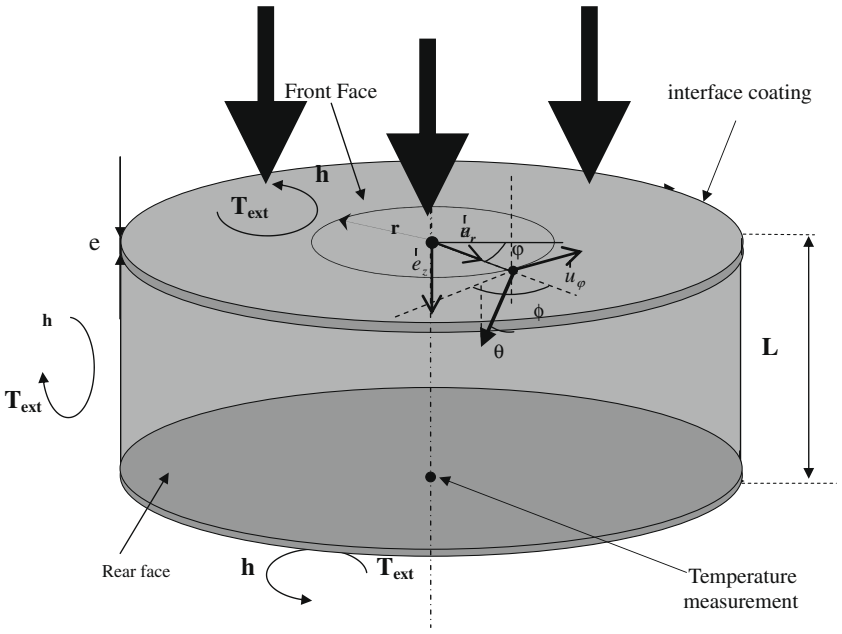

Fig. 1. Representation of the sample and of the coordinate system.

$$\frac{\mu}{r}\frac{\partial(r\cdot I^{\lambda}_{r,z,\vec{\Delta}})}{\partial r}-\frac{1}{r}\frac{\partial(\eta\cdot I^{\lambda}_{r,z,\vec{\Delta}})}{\partial\phi}+\xi\frac{\partial I^{\lambda}_{r,z,\vec{\Delta}}}{\partial z}+\beta_{\lambda}\cdot I_{r,z,\vec{\Delta}} = \kappa_{\lambda}\cdot I^{\lambda}_{0}(T)+\frac{\sigma_{\lambda}}{4\pi}\int_{\Omega'=4\pi}P_{\lambda}(\nu)\cdot I^{\lambda}_{r,z,\vec{\Delta}}\cdot d\Omega' \quad (6)$$

$\eta = \sin\theta\cdot\sin\phi$; $\mu = \sin\theta\cdot\cos\phi$ and $\xi = cos\ \theta$ are the directing cosines; $\nu = \mu\cdot\mu' + \eta\cdot\eta' + \xi\cdot\xi'$ is the cosine of the angle between incident and scattering directions and β_{λ}, κ_{λ}, σ_{λ} and $P_{\lambda}(\nu)$ are the spectral radiative properties.

2.1.1.1. Radiative boundary conditions. At the front and rear faces (see Fig. 1), the boundary conditions of the RTE for emissive and diffusely reflecting interfaces are:

$$I^{\lambda}_{r,z=e,\vec{\Delta}} = \varepsilon^{\lambda}_{coat}\cdot I^{\lambda}_{0}(T_1)+\frac{1-\varepsilon^{\lambda}_{coat}}{\pi}\cdot\int_{\Omega'=2\pi;\xi'<0} I^{\lambda}_{r,z,\vec{\Delta}'}\cdot|\xi'|\cdot d\Omega' \quad \text{for } \xi>0 \quad \text{and} \quad -R_{\max}<r<R_{\max} \quad (7)$$

$$I^{\lambda}_{r,z=L-e,\vec{\Delta}} = \varepsilon^{\lambda}_{coat}\cdot I^{\lambda}_{0}(T_2)+\frac{1-\varepsilon^{\lambda}_{coat}}{\pi}\cdot\int_{\Omega'=2\pi;\xi'>0} I^{\lambda}_{r,z,\vec{\Delta}'}\cdot|\xi'|\cdot d\Omega' \quad \text{for } \xi<0 \quad \text{and} \quad -R_{\max}<r<R_{\max} \quad (8)$$

At the lateral boundaries, we have:

$$I^{\lambda}_{R_{\max},z,\vec{\Delta}} = I^{\lambda}_{0}(T(R_{\max},z)) \quad \text{for } \mu>0 \quad \text{and} \quad e<z<L-e \quad (9)$$

2.1.1.2. Thermal boundary conditions. Before the beginning of the heating, the medium is at a uniform temperature. This temperature is the external temperature and then:

$$\forall r \quad \text{and} \quad z, \quad T(r,z)=T_{ext} \quad \text{at } t=0\ \text{s} \quad (10)$$

During the pulse irradiation by the FLASH (duration τ), the front face of the sample collects a heating power per surface unit $\dot{Q}$. In our numerical model, we assume that this radiative energy is entirely absorbed and that the heat is uniformly generated along its path in the interface coating. Thus, the heat generation could be treated as an internal heat source. We also assume that the heating power is uniformly distributed at the surface of the coating.

At the horizontal interfaces between the coating and the sample ($z = e$ and $z = L - e$), if we neglect the thermal resistance, the heat fluxes balance leads to:

$$-\left(k_{coat}\frac{\partial T_{coat}}{\partial z}\right)_{z=e} = q^{z}_{r}\big|_{z=e}-k_c\frac{\partial T}{\partial z}\bigg|_{z=e} \quad \text{and} \quad -\left(k_{coat}\frac{\partial T_{coat}}{\partial z}\right)_{z=L-e} = q^{z}_{r}\big|_{z=L-e}-k_c\frac{\partial T}{\partial z}\bigg|_{z=L-e} \quad (11)$$

The lateral surface of the sample is also submitted to thermal boundary conditions due to the convective and radiative heat transfer with the external environment. The rate of heat exchange by radiation is equal to $\varepsilon\cdot\sigma_{SB}\cdot(T_s^4-T_{ext}^4)$ and for a relatively small difference $T_s - T_{ext}$, we can consider that: $\varepsilon\cdot\sigma_{SB}\cdot(T_s^4-T_{ext}^4)\approx\varepsilon\cdot\sigma_{SB}\cdot T_s^3\cdot(T_s-T_{ext})$. Thus, the total heat flux exchanged by the lateral surface with the environment could be summarized in a unique coefficient h which takes into account the convective and radiative exchanges: $h = h_{conv} + \varepsilon\sigma_{SB}T_s^3$. If we also assume that the convection coefficients h_{conv} and the temperatures T_s on the horizontal and vertical surfaces are identical, the thermal boundary conditions on these surfaces reduce to:

$$-k_c\left(\frac{\partial T}{\partial r}\right)_{r=R_{\max}} = -h\cdot(T_{R_{\max},z}-T_{ext}) \text{ for the surface defined by } r=R_{\max},\ e<z<L-e \quad (12)$$

$$-k_{coat}\left(\frac{\partial T_{coat}}{\partial r}\right)_{r=R_{\max}} = -h\cdot(T_{coat}|_{R_{\max},z}-T_{ext}) \text{ for } r=R_{\max},\ 0<z<e,\ L-e<z<L, \quad (13)$$

$$-k_{coat}\left(\frac{\partial T_{coat}}{\partial z}\right)_{z=0} = h\cdot(T_{coat}|_{z=0}-T_{ext}) \text{ and } k_{coat}\left(\frac{\partial T_{coat}}{\partial z}\right)_{z=L} = h\cdot(T_{coat}|_{z=L}-T_{ext}) \quad (14)$$

for the surfaces defined by $z = 0$, $0 < r < R_{\max}$ and $z = L$, $0 < r < R_{\max}$, respectively.

2.1.2. Numerical resolution of the transient coupled heat transfer

In order to solve the energy equation and to calculate numerically the variations of the temperature field during the transient heat transfer, we use an explicit time marching technique. When

the time interval Δt between two time steps is small ($\Delta t < 0.1$ s in our study), the temperature field at the new time step could be calculated directly using the radiation intensity field at the previous time step without causing errors. In their study on the temperature rise of a cylindrical glass gob, Viskanta and Lim [22] used the same simplification.

2.1.2.1. Resolution of the energy equation and computation of the temperature field. At each time step, the resolution of the energy equation permits to compute the new temperature distribution from the temperature field and radiation intensity profile at the previous time step. To solve this equation, we use a spatial discretization dividing the volume in $nR \times nZ$ elementary volumes. The discretizations along the z-axis and r-axis differ according to the zone considered. Three different zones are considered:

The interface coatings at the front and back side of the sample delimited by $0 < z < e$ and $0 < r < R_{\max}$ or $L - e < z < L$ and $0 < r < R_{\max}$ for which $\Delta r_i = \frac{R_{\max}}{nR}$ $i = 1, nR$ and $\Delta z_j = \frac{e}{nZ_{coat}}$ $j = 1, nZ_{coat}$The sample delimited by $e < z < L - e$ and $0 < r < R_{\max}$ for which $\Delta r_i = \frac{R_{\max}}{nR}$ and $\Delta z_j = \frac{L-2e}{nZ}$.

The numerical resolution computes the temperature at the center and on the boundary of each volume. At $t = 0$ s, the temperature field is homogeneous and equal to T_{ext}:

$$T^0_{i,j} = T_{coat}\Big|^0_{i,j} = T_{ext} \ \forall i \text{ and } j \tag{15}$$

For the nodes containing the semi-transparent foam and which are not in contact with the coating or lateral boundaries, the temperatures are computed by expressing the energy equation (Eq. (2)) in a discretised form.

Similar relations are obtained for the temperature of the coating nodes in which the radiative flux divergence is null.

For the nodes of foams or coating placed near the coating-foam interface or near the lateral boundaries, similar discretised relations could be obtained by applying energy balance that take into account the thermal boundary conditions (Eqs. (10)–(14)).

Finally, for the coating nodes of the front face placed at the interface with the environment, the discretised relation must also take into account the internal heat generation $S_{i,j}$ due to the pulse irradiation which only occurs when $t < \tau$. This internal heat generation is proportional to the surface area of the node $A_{i,j}$ and to the time step Δt: $S_{i,j} = \dot{Q} \cdot A_{i,j} \cdot \Delta t$.

2.1.2.2. Resolution of the 2-D axisymmetric RTE using the discrete ordinates method. In order to calculate the radiative flux $(\vec{q}_r)_{i,j}$ and the radiative flux divergence $\nabla(\vec{q}_r)_{i,j}$in each point of the spatial discretization, it is necessary to solve the 2-D axisymmetric radiative transfer equation (Eq. (6)) for all the wavelengths participating to the radiative transfer. In the present study, we use the discrete ordinates method based on a spatial discretization of the cylindrical sample and on an angular discretization (discrete directions m (μ_m, η_m, ξ_m) with given weighting factors w_m) of the space. For convenience purpose, the spatial discretization is the same as the one used for the numerical resolution of the energy equation. The 2-D discrete ordinates solution for a radiatively participating medium in a cylindrical enclosure has been widely described, notably by Carlson and Lathrop [23] or Jendoubi et al. [24] and we will not detail it in this article.

Once the discretised intensity field in the semi-transparent medium around the wire has been computed, the radiative fluxes and radiative flux divergences are calculated using the discretised form of Eqs. (9) and (10):

$$(q^r_r)_{i,j} = \left[\sum_{m=1}^{nd} I^m_{i,j} \cdot \mu_m \cdot w_m\right] \quad \text{and} \quad (q^z_r)_{i,j} = \left[\sum_{m=1}^{nd} I^m_{i,j} \cdot \xi_m \cdot w_m\right]. \tag{16}$$

$$\nabla(\vec{q}_r)_{i,j} = \frac{1}{r_i} \cdot \frac{r_{i+1/2} \cdot (q^r_r)_{i+1/2,j} - r_{i-1/2} \cdot (q^r_r)_{i-1/2,j}}{\Delta r_i} + \frac{(q^z_r)_{i,j+1/2} - (q^z_r)_{i,j-1/2}}{\Delta z} \tag{17}$$

2.2. Identification of conductive and radiative properties

The identification procedure developed is based on a list square fit method which minimizes the difference between the temperature $T_{exp.}(t)$ measured at the center of the back side of the irradiated sample during the FLASH experiment and the temperature $T_{num.}(t)$ predicted by the numerical model for given experimental conditions. The principle is to minimize the function F representing the sum of the quadratic discrepancies between the experimental and theoretical variations of the temperature:

$$F = \sum_{n=1}^{N_t} [T_{exp.}(t_n) - T_{num.}(t_n)]^2 \tag{18}$$

The evolution of the temperature calculated by our theoretical model is influenced by the following parameters: L, $R_{\max}$, ρ_{coat}, C_{coat}, $k_{coat,}$ ε_{coat}, h and the thermal properties of the semi-transparent medium. All these parameters are known except the thermal properties of the foam and the coefficient h. Thus, $T_{num.}(t)$ and F only depend on these parameters noted P_k with $k = 1, N$. The choice of these parameters is discussed in Section 2.3. Then, we have:

$$F = F(P_1, \ldots, P_N) = \sum_{n=1}^{N_t} [T_{exp.}(t_n) - T_{num.}(P_1, \ldots, P_N)]^2 \tag{19}$$

In order to minimize F, the parameters P_k should satisfy the relations:

$$\frac{\partial F}{\partial P_k} = \frac{\partial}{\partial P_k}\left[\sum_{n=1}^{N_t} (T_{exp.}(t_n) - T_{num.}(t_n))^2\right] = 0 \Rightarrow \sum_{n=1}^{N_t}\left[(T_{exp.}(t_n) - T_{num.}(t_n)) \cdot \frac{\partial T_{num.}(t_n)}{\partial P_k}\right] = 0 \quad \text{for } k = 1, N \tag{20}$$

The partial derivatives $\frac{\partial T_{num.}(t_n)}{\partial P_k}$ are called the sensibility coefficients and represent the rate of variation of the temperature at the center of the back side at the time t_n due to a variation of the parameters $P_{k.}$

In order to solve this system of non-linear equations, we use the iterative method of Gauss starting from initial values P^0_k. At each iteration level l, the following system of equations is solved:

$$\sum_{n=1}^{N_t}\left[(T_{exp.}(t_n) - (T_{num.}(t_n))^l) \cdot \left(\frac{\partial T_{num.}(t_n)}{\partial P_k}\right)^l\right] = 0 \quad \text{for } k = 1, N \tag{21}$$

Moreover, the value $(T_{num.}(t_n))^l$ at the iteration level l can be approximated from the values at the iteration level $l-1$ by the following relation:

$$T_{num.}\left(t_n, [P_k]^l_{k=1,N}\right) = T_{num.}\left(t_n, [P_k]^{l-1}_{k=1,N}\right) + \sum_{k=1}^{N}\left(\frac{\partial T_{num.}(t_n)}{\partial P_k}\right)^{l-1} \cdot \Delta P^{l-1}_k \tag{22}$$

We finally have to solve the following matrix system, where the superscript l refers to the entire matrixes:

$$[A_{kj}]^l \cdot [\Delta P_j]^l = [B_k]^l \quad \text{with}$$

$$A^l_{kj} = \sum_{n=1}^{N_t} \left(\frac{\partial T_{num.}(t_n)}{\partial P_k} \right)^l \cdot \left(\frac{\partial T_{num.}(t_n)}{\partial P_j} \right)^l;$$

$$B^l_k = \sum_{n=1}^{N_t} \left((T_{exp.}(t_n) - T_{num.}(t_n)) \cdot \frac{\partial T_{num.}(t_n)}{\partial P_k} \right)^l \quad (23)$$

This system is solved successively for each iteration level l to calculate the values $[P^{l+1}_k = P^l_k + \Delta P^l_k]_{k=1,N}$ until the ratios $\left[\frac{\Delta P^l_k}{P^l_k}\right]_{k=1,N}$ are lower than a convergence criterion.

2.3. Choice of the conductive and radiative parameters to identify

The model developed is relatively comprehensive and allows theoretically an accurate simulation of the temperature rise at the rear side of the semi-transparent sample. However, its main drawback stems from the fact that it requires a high number of unknown thermal parameters which is prohibitive if ones would like to implement an identification process. Indeed, in addition to the thermal conductivity k_c, the extinction coefficient, the scattering albedo and the scattering phase function have to be known, a priori, for all the wavelengths. That is the reason why we investigated the possibility to reduce the number of parameters characterizing the radiative heat transfer without degrading the accuracy of the model.

A first simplification would be to use global radiative properties defined for the entire wavelength range of interest instead of numerous spectral values. This simplification does not imply necessary that the radiative properties of the foams are independent of the radiation wavelength but rather that, for each foam, there exists unique values of the extinction coefficient, scattering albedo and scattering phase function that accurately simulate the global radiative behavior of the material in the entire wavelength range. By this manner, a global extinction coefficient, albedo and scattering phase function are sufficient to characterize the interaction of the material with thermal radiation. Another simplification is to consider that the foam material scatter radiation isotropically. Under these two assumptions, the radiation-sample interaction could be reproduced using two properties: the extinction coefficient and albedo of the grey isotropically scattering semi-transparent material that best match the radiative thermal behavior of the foam. This two scaled parameters are noted β^* and ω^*. To avoid any misunderstanding, we remind that the objective of the present work is to identify simplified properties which are able to describe the conductive and radiative heat transfer of the samples tested but not necessarily their entire exact radiative behavior. For instance, it is possible that the use of the identified properties β^* and ω^* to simulate the directional transmittance and reflectance of a slab of foam submitted to an incident plane wave, might lead to noticeable differences in the angular and spectral distributions. However, we will see that that the aim of the simplified representation of the radiative transfer retained is fulfilled as it permits to reproduce satisfactorily the 1-D transient and steady-state heat transfer. The only drawback of the simplified parameters is that for heat transfer with large temperature gradients, it may be necessary to have a set of variations of these properties in the range of temperatures considered rather than unique values. In summary, three parameters are sufficient to predict the thermal behavior of the samples tested and a total of four parameters permit to reproduce the FLASH experiment: $P_1 = h$, $P_2 = k_c$, $P_3 = \beta^*$ and $P_4 = \omega^*$.

In order to check that the simplified model retained is able to describe accurately the thermal behavior of solid foams, we have computed the theoretical thermograms for fictitious but realistic semi-transparent non-grey and non-isotropically scattering materials simulating solid foams. Thereafter, we applied our identification procedure (four parameters) to these theoretical thermograms in order to estimate the thermal conductivity k_c, the extinction coefficient β^* and the albedo ω^* of the corresponding grey isotropically scattering material having the same other physical properties C and ρ. To simulate a realistic case, we used the radiative properties measured by Loretz et al. [11] for NiCrAl and FeCrAl foams. The authors give the variations, with the wavelength, of the extinction coefficient β_λ, scattering albedo ω_λ and of the parameter of specularity S_λ describing the repartition of the energy scattered. S_λ actually represents the proportion of rays reflected specularly. Thus, the phase function and the asymmetry parameter $\langle\mu\rangle_\lambda$ of the foam sample are directly related to S_λ: $P_\lambda(\theta) = S_\lambda + (1 - S_\lambda) \cdot \frac{8}{3\pi} \cdot (\sin\theta - \theta \cdot \cos\theta)$, $\langle\mu\rangle_\lambda \approx (1 - S_\lambda) \times 0.444$. The variations of β_λ, ω_λ and S_λ are illustrated in Fig. 2a. We used the S_6 quadrature and a grey per band model with 27 bands of wavelengths. The other properties have been chosen in order to be representative of a real metal foam: $k_c = 0.2$ W/m/K, $\rho = 500$ kg/m^3, $C = 500$ J/kg/K, $L = 10.2$ mm. The properties of the interface coating are: $e = 0.3$ mm, $C_{coat} = 1200$ J/kg/K, $\rho_{coat} = 1000$ kg/m^3 and $k_{coat} = 3.3$ W/m/K. The computations were conducted for an initial temperature $T_{init} = 673$ K and with a convective heat transfer coefficient $h = 5$ W/m^2/K. The values of the four parameters identified by our procedure for the two fictive foams are:

- NiCral foam: $\beta^* = 866.5$ m^{-1}; $\omega^* = 0.783$, $k_c = 0.204$ W/m/K and $h = 5.004$ W/m^2/K.
- FeCral foam: $\beta^* = 463.06$ m^{-1}; $\omega^* = 0.779$, $k_c = 0.2014$ W/m/K and $h = 4.999$ W/m^2/K.

We can check the coherence of the simplified properties β^* and ω^* identified by comparing them with weighted extinction coefficients $\tilde{\beta}$ and weighted albedos $\tilde{\omega}$ which take into account the anisotropic scattering and thus, have the same signification. They are defined by

$$\tilde{\beta} = \kappa + \tilde{\sigma}; \quad \tilde{\omega} = \tilde{\sigma}/\tilde{\beta} \quad \text{with} \quad \kappa = (1 - \omega) \cdot \beta; \quad \sigma = \omega \cdot \beta;$$

$$\tilde{\sigma} = \sigma(1 - \langle\mu\rangle) \quad \text{and} \quad \langle\mu\rangle = \frac{1}{2} \int_{-1}^{1} P(\mu) \cdot \mu \cdot d\mu$$

In the case of the NiCrAl foam simulated, if we assume that the radiative properties β_λ, ω_λ and g_λ (Fig. 2a) are almost independent of wavelength and equal to ≈ 656 m^{-1}; $\omega \approx 0.7$ and $g \approx 0.15$ (Planck averaged values in the range of wavelength [1.7–25] μm), we obtain: $\kappa \approx 197$ m^{-1}; $\sigma \approx 459$ m^{-1}; $\langle\mu\rangle \approx -0.45 \Rightarrow \langle\mu\rangle \approx -0.45\tilde{\sigma} \approx 665$ m$^{-1} \Rightarrow \tilde{\beta} \approx 863$ m$^{-1} \Rightarrow \tilde{\omega} \approx 0.77$.

Similarly, for the FeCrAl foam, if we assume that the radiative properties are almost independent of wavelength (Fig. 2a; ≈ 416.5 m^{-1}; $\omega \approx 0.77$ and $g \approx 0.68$) we obtain: $\kappa \approx 96.3$ m^{-1}; $\sigma \approx 320$ m^{-1}; $\langle\mu\rangle \approx -0.169 \Rightarrow \tilde{\sigma} \approx 374$ m$^{-1} \Rightarrow \tilde{\beta} \approx 470m^{-1} \Rightarrow \tilde{\omega} \approx 0.795$.

These values are quite close to the properties identified ($\beta^* = 866.5$ m^{-1}; $\omega^* = 0.783$ for NiCrAl and $\beta^* = 463.06$ m^{-1}; $\omega^* = 0.779$ for FeCrAl). This tends to confirm that the simplified model retained is coherent.

The comparisons of the thermograms obtained for the foams (Th. NiCrAl or FeCrAl) and for the corresponding grey materials (ident. NiCrAl or FeCrAl) and the evolution of the relative discrepancy due to the simplifications ($discrep. = |T_{th.}(t_i) - T_{ident.}(t_i)|$) are illustrated in Fig. 2b. In order to better grasp the influence of each parameter, we also illustrate in Fig. 2c the evolutions of the dimensionless sensibility coefficients $\frac{\partial T_{num.}(t_n)}{\partial P_k} \cdot P_k$ obtained at the last iteration of the identification for the fictive NiCrAl foam.

First, one can remark that the thermograms obtained for the semi-transparent materials are noticeably different from classical thermograms on purely conductive materials, especially at the beginning of the measurement and notably for the FeCrAl foam. Indeed, the increase of the temperature occurs noticeably sooner

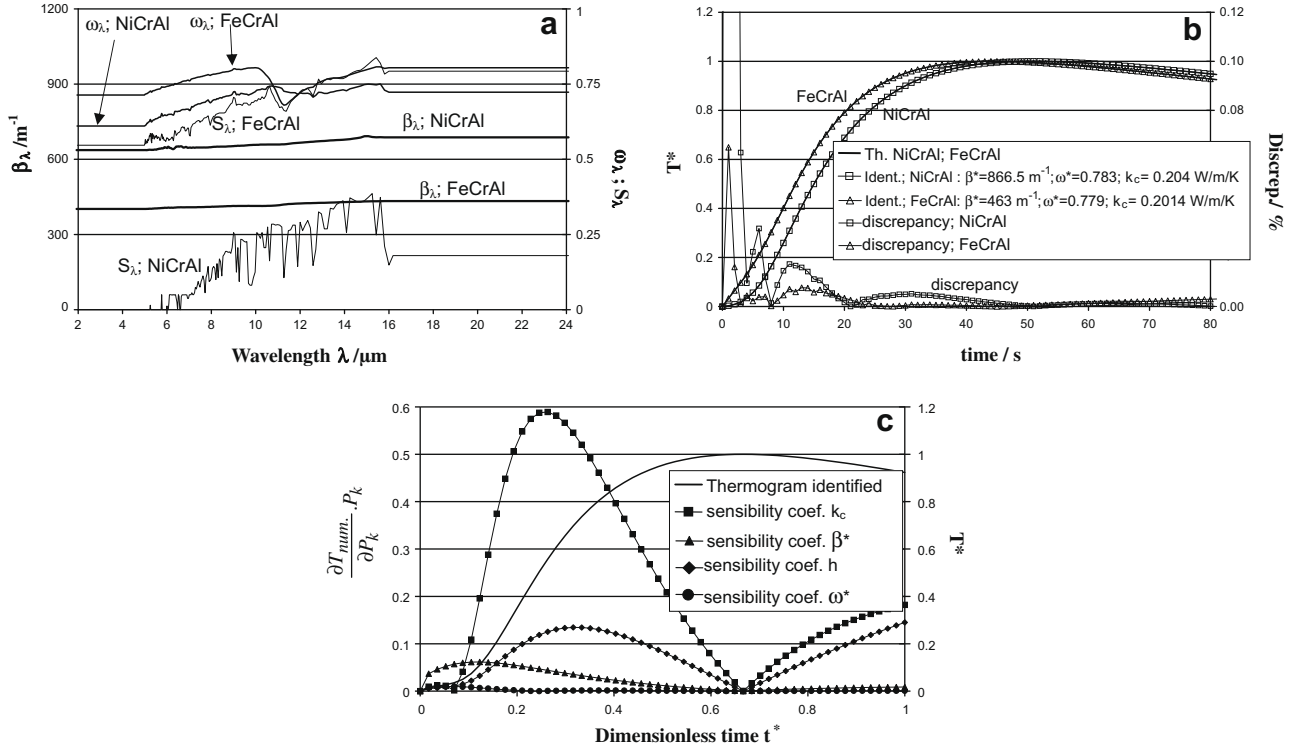

Fig. 2. (a) Evolution of the spectral radiative properties used for the simulation of the FLASH measurement. (b) Comparison of the theoretical thermograms obtained for the NiCrAl and FeCrAl foams and for the associated grey isotropically scattering media. (c) Evolution of the dimensionless sensibility coefficients for the fictive NiCrAl foam.

than when the heat transfer is purely conductive. These differences are due to the radiative transfer which propagates quasi instantaneously through the sample. At this temperature, the radiative contribution is predominant, particularly for the FeCrAl foam which is more transparent to radiation.

One can also observe that the thermograms computed for the corresponding grey isotropically scattering materials match very well the thermograms computed from the realistic spectral variations of the radiative properties of NiCrAl and FeCrAl foams. In both cases, the relative error gets lower than 1% after 3 s and lower than 0.1% after only 5 s. It can also be noted that the values of k_c and h identified are very close to the original values used for the fictive measurement. This means that the differences on the transient heat transfer due to the simplifications of the radiative heat transfer are not counterbalanced by deviations of the other identified parameters. This clearly shows that the radiative behavior of materials with spectrally varying properties during a FLASH measurement could be matched very well by an "equivalent" grey and isotropically scattering semi-transparent medium (only two radiative properties) having the same thermal conductivity.

However, one have to keep in mind that conductive and radiative properties of foams are generally wanted so as to estimate heat fluxes passing through these foams. So, one has to check that the thermal properties identified permit not only to reproduce the FLASH thermogram accurately but also to give an accurate estimation of the total heat flux traveling through the sample. Then, in order to be sure that the three thermal parameters retained (k_c, β^*; ω^*) are sufficient to entirely characterize the foam, we have computed, in both cases (FeCrAl and NiCrAl), the equivalent thermal conductivities of the foams and of the associated grey materials. The computation were conducted by solving simultaneously the steady-state energy equation and radiative transfer equation in a 1-D planar slab (thickness $L = 0.05$ m) subjected to a temperature gradient ($T = 673$ K; $\Delta T = 10$ K). The methods of resolution are those described previously (Section 2.1.2). The equivalent conductivities computed are: 0.3131 and 0.3082 W/m/K for the NiCrAl foam and the associated grey material and 0.3905 and 0.3915 W/m/K for the FeCrAl foam and the associated grey material. This corresponds to relative errors of 1.5% and 0.25%, respectively, which are quite negligible.

Consequently, we can conclude that it is possible to summarize faithfully the thermal radiative behavior of foams submitted to transient or steady-state heat transfer in only two radiative parameters: β^* and ω^*. Three parameters are sufficient to characterize the global thermal behavior: k_c, β^* and ω^*. This strong reduction of the number of parameters leads to an identification procedure allowing to characterize entirely the thermal heat transfer in the FLASH sample with only four parameters.

Finally, as regards the evolution of the dimensionless sensibility coefficients, one can remark that the thermogram is mostly influenced by the effective conductivity of the sample. However, the maximum values of the dimensionless sensibility coefficients of β^* and h are the same order of magnitude as that of k_c. On the other hand, the dimensionless sensibility coefficient of the scaled albedo is noticeably smaller. Thus, we can expect a rather good estimation of k_c, β^* and h. But the uncertainty on the value of ω^* identified will certainly be noticeably more important. We also notice that the influences of the radiative parameters are especially important at the beginning of the measurement when the influence of k_c and h is almost null. The dimensionless sensibility coefficients of k_c and h get more important at intermediate times and at large times.

3. Experimental investigation

3.1. Foam samples

Four types of metal or ceramic foams have been tested. They are made of Ni–Cr alloy, fecralloy (Fe 72.8/Cr 22/Al 5/Y 0.1/Zr 0.1) mullite ($Al_6Si_2O_{13}$) and zirconia (ZrO_2) partially stabilized with

Table 1
Properties of the metallic and ceramic foam samples characterized experimentally.

Sample No.	Solid phase	ρ (kg/m3)	D_{cell} (mm)	ε	C (J/kg/K)	L (mm) ss revet	L (mm) av revet
1	Ni–Cr–Al 1	537	1.4	0.937	501	10.2	10.2
2	Ni–Cr–Al 2	503	1.2/0.6	0.941	501	10.52	10.8
3	Ni–Cr–Al 3	587	0.8/0.4	0.931	501	5.31	5.8
4	Ni–Cr–Al 4	665	2.8/1.4	0.922	501	7.34	8
5	Fecralloy 1–1	230	60PPI 0.423 m	0.9682	487	9.05	9.4
6	Fecralloy 1–2	230	60PPI 0.423 m	0.9681	487	9.35	9.9
7	Fecralloy 2–1	253	80PPI 0.32 mm	0.9649	487	10.35	10.7
8	Fecralloy 2–2	270	80PPI 0.32 mm	0.9627	486	8.3	9.2
9	Mullite	534	1.2	0.809	950	11.05	11.5
10	Zirconia	966	1.2	0.832	451	10.55	10.6

yttria (Y_2O_3), noted PsZ. The thermal properties of these bulk materials are given in Table 1. The foam manufacturers indicated that the foam samples are almost isotropic, which have been confirmed by SEM image analysis. So, our identification procedure is applicable. The experimental investigations have been conducted at three different temperatures: ambient temperature (296 K) and high temperatures (433 and 673 K).

The porosities of the samples have been estimated from the measurements of their mass M (kg) and volume V (m^3):

$$\varepsilon = \frac{\rho_{solid} - M/V}{\rho_{solid} - \rho_{air}} \tag{24}$$

The measured densities and porosities of all the samples tested are regrouped in Table 1 where we also indicate the mean cell diameter D_{cell} provided by the manufacturer and the specific heat C which is estimated by

$$C = \frac{\varepsilon\rho_{air}C_{air} + (1-\varepsilon)\rho_{solid}C_{solid}}{\rho} \tag{25}$$

This specific heat is assumed independent of the temperature for the 10 samples.

3.2. Experimental apparatus

For the measurements at ambient temperature, we used a classical FLASH apparatus composed of a sample holder of 30 mm in diameter and FLASH lamps of short thermal pulse ($T < 10$ ms).

At high temperatures, we used a special set-up already described in reference [25]. It consists essentially of an inductive furnace, a resistive furnace and a laser-FLASH diffusivimeter measuring the temperature rise at the rear face of the sample. It allows to conduct experimental measurements up to 3300 K in gaseous (helium, nitrogen and argon) or vacuum environments. FLASH experiments can be performed in the two furnaces, by using the same laser. Depending on the test temperature, one furnace or the other are used to heat the specimen. The sample is placed in a furnace and heated at a uniform temperature. For thermal diffusivity measurements performed between 300 and 1300 K, the specimen (30 mm in diameter and about 1–10 mm thick) is put vertically in the resistive furnace. For

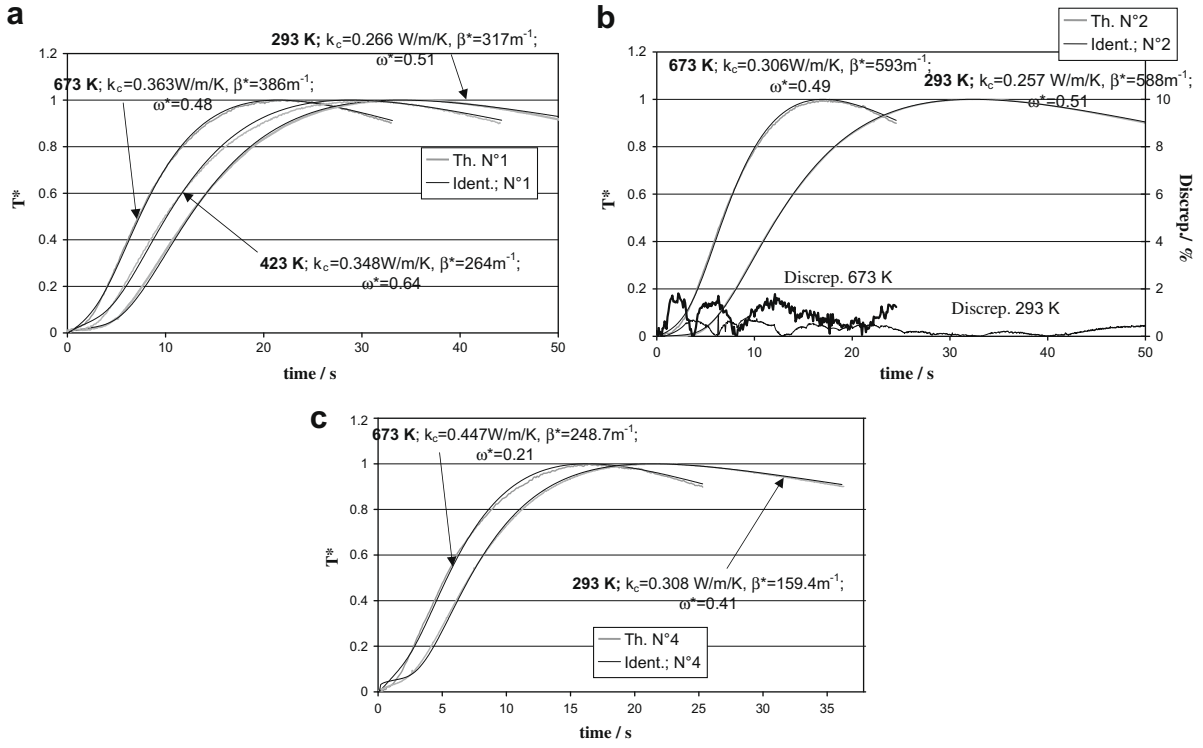

Fig. 3. (a) Comparison of the experimental and numerical thermograms for sample No. 1. (b) Comparison of the experimental and numerical thermograms for sample No. 2. (c) Comparison of the experimental and numerical thermograms for sample No. 4.

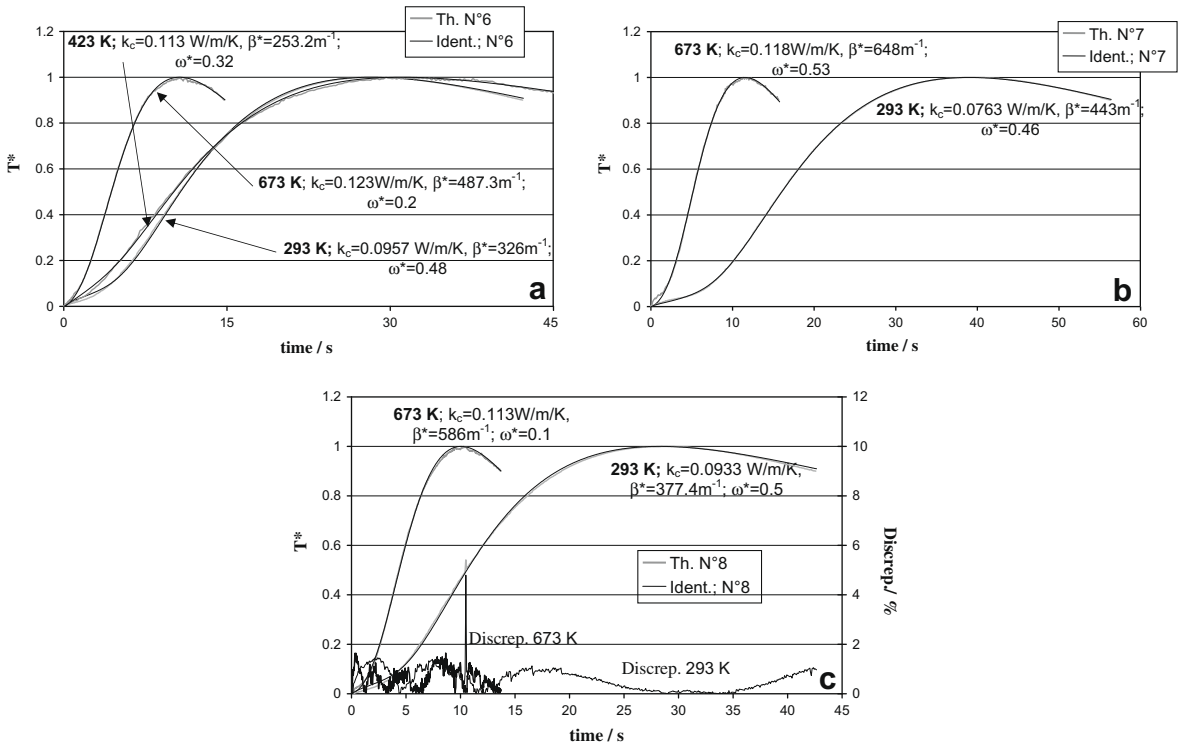

Fig. 4. (a) Comparison of the experimental and numerical thermograms for sample No. 6. (b) Comparison of the experimental and numerical thermograms for sample No. 7. (c) Comparison of the experimental and numerical thermograms for sample No. 8.

very high temperature measurements (600–3000 K), it is put horizontally on the top of the graphite susceptor, inside the inductive furnace. The source used to irradiate the front face of the specimen is a Nd:phosphate glass laser, having a wavelength of 1054 nm and a pulse duration around 450 μs. A flat mobile mirror, situated at the beginning of the laser path, allows directing the beam to one or the other furnace. It is then transmitted to the inductive furnace or the resistive one by a set of lenses and mirrors so that its diameter varies approximately from 10 to 20 mm on the specimen.

The induced temperature rise on the rear face of the specimen is measured by optical way with two infrared detectors, HgCdTe detector for the temperature range [300–1300 K] and InGaAs detector for the range [1100–3300 K].

3.3. Experimental results

3.3.1. Presentation and discussion on the experimental results

The identification procedure developed have been applied to the thermograms measured at ambient temperature ($T = 296$ K) and at $T = 433$ K or $T = 673$ K for the 10 foam samples. However, the quality of some thermograms obtained at high temperatures was not sufficient to obtain satisfying identifications. The values of the parameters after identification as well as the mean relative discrepancy $\langle discrep. \rangle$ between the experimental thermograms and the temperature rise predicted by the numerical model after identification are summarized in Table 2. The mean discrepancy is defined by: $\langle discrep. \rangle = \langle |T_{exp.}(t) - T_{ident.}(t)| \rangle_{t=0 \to \Delta t}$. The comparisons between the measured thermograms and the thermograms obtained after identification of the corresponding grey materials are illustrated in Figs. 3(a, b and c for NiCrAl foams), 4(a, b and c for FeCrAl foams) and 5(a and b for mullite and PsZ foams) for sample Nos. 1, 2, 4, 6–10.

As illustrated on these figures, we can note that our simulation using the global equivalent radiative properties β^* and ω^* combined with the identification procedure permits to match the evolution of the temperature very well for all the samples tested since the average discrepancy between experimental and theoretical thermograms is always lower than 1%.

The analysis of the results illustrated in Table 2 leads to several remarks for each type of foam:

- For NiCrAl foams (sample Nos. 1–4), the properties identified show a noticeable increase of the thermal conductivity k_c with the temperature. This increase is observed for all the samples tested. It is most likely due to an increase of the thermal conductivities of the bulk material (NiCrAl) and of air with the temperature since the porous morphology of the foams does not change with temperature. Literature data concerning the bulk thermal properties of NiCrAl [26] confirm this assumption. The increase of k_c with T is relatively important as it can reach 45% for sample No. 4 between ambient temperature and 673 K. For the other samples, the increase is less pronounced. The conductive properties identified also indicate a global increase of the effective conductivity with the density of the samples considered except for sample No. 3 for which the thermal conductivity is lower than sample Nos. 1 and 2 although its density is more important. This global increase of k_c with the density is consistent with theoretical conclusions of previous studies [7] which underlined the substantial influence of the volume fraction of highly conductive solid phase on the conductive heat transfer. The surprising results evocated for sample No. 3 might be explained by a noticeable difference in the porous structure between this foam and the other samples. Indeed, Coquard et al. [7] have already shown that the shape of the struts forming the cellular materials could have a noticeable influence on the magnitude of conductive heat transfer.

As regards the radiative properties, the comparison of the values of β^* identified for the different samples show that the radiation-matter interaction strongly depends on the cell diameter.

Table 2
Thermal properties identified for the metallic and ceramic foam samples.

Sample No.	T (K)	k_c (W/m/K)	β^* (m−1)	ω^*	⟨*discrep.*⟩ (%)	k_{equ} (W/m/K)	k_c/k_{equ} (%)
1	296	0.266	317	0.51	0.73	0.289	92.0
	423	0.348	264	0.64	1.08	0.428	81.3
	673	0.363	386	0.48	0.71	0.590	61.5
2	296	0.257	587.6	0.49	0.28	0.270	95.2
	673	0.306	593	0.51	0.882	0.457	67.0
3	296	0.246	734	0.71	0.47	0.256	96.0
4	296	0.308	159.4	0.41	0.687	0.352	87.5
	673	0.447	248.6	0.21	1.20	0.792	56.4
5	296	0.0980	315	0.56	0.603	0.1215	80.7
6	296	0.0957	325.8	0.48	0.475	0.1185	80.8
	423	0.113	253.2	0.32	0.6498	0.197	57.4
	673	0.123	487.3	0.2	0.431	0.305	40.3
7	296	0.0763	443.2	0.46	0.164	0.0933	81.8
	673	0.1181	648	0.5	0.557	0.256	46.1
8	296	0.0933	377.4	0.5	0.564	0.113	82.6
	673	0.113	586	0.1	0.644	0.265	42.6
9	296	0.279	374.7	0.2	0.560	0.299	93.3
	673	0.2985	355.6	0.49	0.769	0.544	54.9
10	296	0.257	324.5	0.29	0.538	0.280	91.8
	423	0.294	351	0.31	0.666	0.356	82.6
	673	0.265	371.6	0.2	0.747	0.501	52.9

Indeed, the equivalent extinction coefficient is very large for sample No. 3 with noticeably small cells and very weak for sample No. 4 with large cells whilst their other properties (density, optical properties of the bulk material) are almost identical. Besides, if we also consider the results for sample Nos. 1 and 2, it seems that β^* is directly proportional to the inverse of the mean cell diameter indicated by the manufacturer. These remarks are consistent with the theoretical conclusions drawn by Zhao et al. [13] or Wang and Pan [15] on the radiative properties and with the previous experimental investigations [16] on the radiative conductivity of FeCrAl foams. This influence could be simply explained by the fact that, for a given porosity, if the diameter of the cells increases, the distance traveled by thermal radiation emitted by the solid phase before being intercepted (mean free path of photons) is more important. Now, the extinction coefficient is directly proportional to the inverse of the mean free path of photons. It is also important to note that the porosity of the foam has a noticeably weaker influence on the radiation-matter interaction than the cell diameter as sample No. 4 is the most transparent to radiation. Finally, we can also compare the global extinction coefficient obtained by our method for sample No. 1 with the one measured by Gauthier [26] on the same sample. The author identified the spectral extinction coefficient, albedo and asymmetry parameter of sample No. 1 from directional and hemispherical transmittances and reflectances measurements made on a slab of foam. Thereafter they computed the scaled extinction coefficient and albedo by averaging the spectral values using the Planck function. They obtained a scaled extinction coefficient, independent of the temperature and equal to 590 m^{-1}. This extinction coefficient is overestimating our measurements. However, our results show that β^* is somewhat independent of the temperature which agrees well with the conclusion of [26].

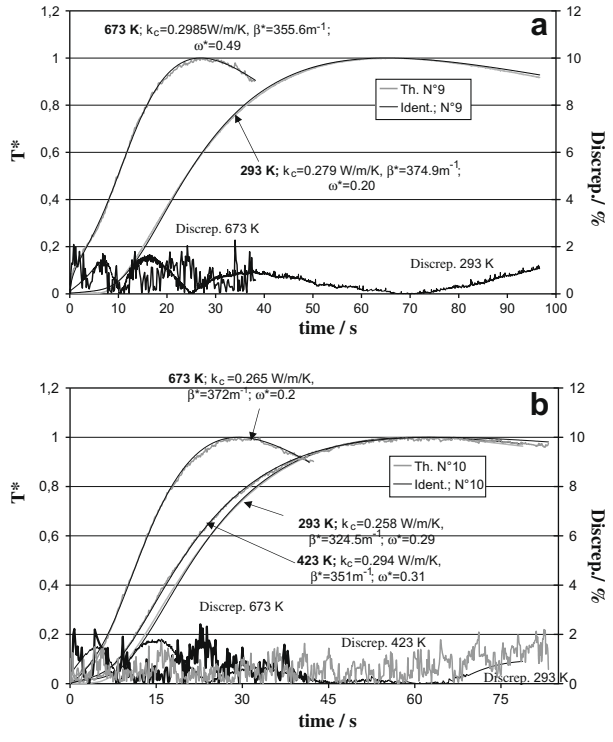

Fig. 5. (a) Comparison of the experimental and numerical thermograms for sample No. 9 (Mullite). (b) Comparison of the experimental and numerical thermograms for sample No. 10 (PsZ).

Concerning the variations of the equivalent scattering albedo ω^*, it is not possible to draw general trends. The values identified are globally comprised between 0.2 and 0.7. Actually, as explained by Loretz et al. [11], this property is mainly related to the optical characteristics of the solid phase (NiCrAl) and to the roughness of the solid surfaces. Therefore, the differences observed between the different NiCrAl samples may be due to differences in the surface state. Moreover, we have seen (Section 2.3) that ω^* has a relatively weak dimensionless sensibility parameter, that is to say that the uncertainty on the value of ω^* identified is relatively important and could be at the origin of the discrepancies observed between the different samples. For sample No. 1, we can compare the values of ω^* obtained at the different temperatures with the experimental results of Gauthier [26] which showed that the glo-

bal albedo of sample No. 1 is independent of temperature (grey behavior) and close to 0.6. Thus, our identified albedo are in good accordance since the values identified does not vary significantly with temperature and are the same order of magnitude.

Finally, concerning the variation of the radiative properties of NiCrAl foams with temperature, it seems that the equivalent extinction coefficient slightly increases between $T = 296$ K and $T = 673$ K. This general trend is observed for sample Nos. 1, 2 and 4. Surprisingly, for sample No. 1, we also remark that β^* slightly decreases when T goes from 296 to 423 K. However, globally, the variations of β^* with T are very limited so that we can consider the global equivalent extinction coefficient β^* practically independent of T. That is to say that the spectral extinction coefficient is independent of the radiation wavelength under consideration. This agrees well with the results presented in [26] which show that the radiative properties of sample No. 1 could be considered as grey. This is also coherent with theoretical conclusions drawn, notably by Loretz et al. [11], which explained that, under geometric optics approximation (which is the case here since $D_{cell} >> \lambda$), the spectral coefficients does not vary with the wavelength.

- For FeCrAl foams (sample Nos. 5–8), we also observe the increase of k_c with the temperature for all the samples tested. Like for NiCrAl foams, this increase is most likely due to an increase of the conductivities of the solid (FeCrAl) and fluid (air) phases. Surprisingly, the effective conductivities of sample Nos. 5 and 6, which are the lightest foams, are more important than for sample Nos. 7 and 8. This conclusion appears to be in contradiction with theoretical conclusions. It seems that k_c could not be related to the porosity of the foam simply. Actually, like for NiCrAl foams (sample No. 3), this surprising result is certainly due to noticeable differences between the porous morphologies of sample Nos. 5 and 6 (60 PPI) and sample Nos. 7 and 8 (80 PPI).

As regards the radiative properties, the conclusions are almost identical to NiCrAl foams. Indeed, one can observe that, for a given temperature, the equivalent extinction coefficients of sample Nos. 7 and 8 having 80 Pores per inch ($D_{cell} \approx 0.31$ mm) are more important than for sample Nos. 5 and 6 with 60 Pores per inch ($D_{cell} \approx 0.42$ mm). This confirms that the cell diameter is a key parameter for the radiation-matter interaction. We also remark, like for NiCrAl foams, the increase of β^* with the temperature between ambient temperature and $T = 673$ K whatever the sample considered. However, for FeCrAl foams, this increase is more pronounced. This observation seems not consistent with theoretical conclusions which predict a spectral extinction coefficient constant for all the I.R radiation wavelengths and thus a global extinction coefficient independent of the temperature. However, one has to keep in mind that the parameter β^* does not actually represent an extinction coefficient but a global parameter encompassing all the phenomenon influencing the propagation of radiation. Finally, like for NiCrAl foams, it is not possible to deduce a general trend for the variations of the scattering albedo with the samples considered. For FeCrAl foams, it is globally comprised between 0.1 and 0.6 and the discrepancies are most likely due to differences in the surface state of the different samples.

- For both mullite and zirconia (PsZ) foams, one can observe a weak increase of the effective thermal conductivity with temperature between ambient temperature and $T = 673$ K. This is consistent with literature data [27–31] concerning dense mullite and dense PsZ which generally mention slight increases of their thermal conductivities with temperature.

Moreover, we observe, for the two foams, that the equivalent extinction coefficients are almost independent of the temperature considered like for NiCrAl foams. It is also important to note that the magnitude of the equivalent extinction coefficients is similar for the two foams. Finally, the only difference regarding the evolution of the thermal characteristics concerns the scattering albedo. Indeed, for zirconia sample ω^* is practically the same for the three temperatures studies whereas, for mullite foam, it varies relatively strongly between ambient and $T = 673$ K. These differences in the variations of ω^* are probably related to differences in the spectral optical properties of the two different solid phases. Moreover, as mentioned previously, the uncertainty on ω^* identified is relatively important.

As for sample No. 1, the radiative properties of the mullite foam (sample No. 9) have also been measured by Gauthier [26] using the same approach. Gauthier shows that, contrary to the NiCrAl sample (sample No. 1), the radiative behavior of sample No. 9 varies noticeably with the wavelength considered since the global albedo increases from approximately 0.25 to 0.65 between $T = 300$ K and $T = 600$ K. These variations are in good accordance with our results which also show a regular increase of ω^* with temperature between 0.2 ($T = 296$ K) and 0.49 ($T = 623$ K). As regards the scaled extinction coefficient, its variation with the temperature measured by Gauthier [26] are slower: 700 m^{-1} at $T = 300$ K and 750 m^{-1} at $T = 600$ K. One can remark that, like for sample No. 1, these values overestimates our results noticeably.

In conclusion, the thermal properties obtained from our identification procedure are coherent as they match satisfactorily the general trends underlined by previous studies. Indeed, the experimental results show the influence of the temperature on the effective thermal conductivities of metal foams due to the increase of the thermal conductivity of the dense solid phase. Moreover, the major influence of the cell diameter on the radiative behavior is also underlined by our investigations.

The thermal properties obtained could be used to evaluate simply the relative importance of the radiative and conductive contributions to the heat transfer according to the temperature. Notably, this would permit to evaluate whether the hypothesis of purely conductive heat transfer is valid for this kind of material at ambient temperature or not. In order to illustrate the importance of both modes of heat transfer, we have computed the equivalent thermal conductivities of each sample at different temperatures with the following characteristics: $L = 0.05$ m, black boundaries, $\Delta T = 10$ K. The equivalent thermal conductivities computed as well as the ratio k_c/k_{equ} representing the contribution of conductive heat transfer are illustrated in Table 2. One can remark that, for NiCrAl, mullite and zirconia foams, the hypothesis of purely conductive heat transfer is acceptable at ambient temperature since more than 92% of the heat is transferred by conduction. On the other hand, for the four FeCrAl foams studied this proportion is approximately 80% and the pure conduction simplification could no more be used without generating noticeable errors.

4. Conclusions

The characterization of the thermal behavior of two-phase material is a hard task especially when, in addition to conductive heat transfer, radiation heat transfer also occurs like in high-porosity metallic and ceramic foams. Classical methods of measurements of the heat transfer generally fail to distinguish the conductive and radiative contributions to the heat transfer in this kind of material. As a matter of fact, they give a unique measured parameter characterizing conductive and radiative heat transfer globally. Thus, this parameter is only valid for the conditions in which the experiment is conducted.

To overcome this limitation, we have proposed a new identification procedure using the experimental devices required in classical

FLASH measurements. A FLASH experiment is applied to the sample considered. Then, an identification procedure allows estimating the conductive and radiative characteristics of the semi-transparent material whose theoretical FLASH response best match the temperature rise measured. The method requires a direct model simulating faithfully the transient heat transfer in a semi-transparent material. As a matter of course, the model should theoretically takes into account a large number of thermal properties especially for the radiative heat transfer which is prohibitive for the identification procedure. However, we show that the use of only three thermal characteristics (one for conduction and two for radiation) is theoretically sufficient to summarize satisfactorily the thermal behavior of solid foams submitted to transient or steady-state heat transfer. These parameters are the effective conductivity k_c of the foam and the extinction coefficient β^* and scattering albedo ω^* of the equivalent grey isotropically scattering semi-transparent medium.

Thereafter, we applied the identification to the FLASH thermograms obtained for several NiCrAl, FeCrAl, mullite and zirconia foams with various properties at different temperatures. We have analyzed the results obtained. The evolutions of the thermal properties with the characteristics of the foams (density, cell diameter, etc.) and with the temperature agree well with the theoretical conclusions of previous studies conducted on this subject. Thus, our measuring procedure proves to be an interesting tool and a noticeable improvement for scientific requiring an accurate and rapid modeling of the thermal behavior of the solid foams. Indeed, it permits to characterize simultaneously the radiative and conductive contributions to heat transfer from a unique experiment.

References

[1] M.A. Schuetz, L.R. Glicksmann, Heat Transfer in Foam Insulation, S.B. Massachusetts Institute of Technology, Cambridge, Department of Mechanical Engineering, December 1982.

[2] L.R. Glicksmann, M.A. Schuetz, in: N.C. Hilyard, Low Density Cellular Plastics, A. Cunningham Chapman Hall, London, 1994, pp. 104–152.

[3] K. Boomsma, D. Poulikakos, On the effective thermal conductivity of a three dimensionally structured fluid saturated metal foams, Int. J. Heat Mass Transfer 44 (4) (2001) 827–836.

[4] A. Bhattacharya, V.V. Calmidi, R.J. Mahajan, Thermophysical properties of high porosity metal foams, Int. J. Heat Mass Transfer 45 (5) (2002) 1017–1031.

[5] A.M. Druma, M.K. Alam, C. Druma, Analysis of thermal conduction in carbon foams, Int. J. Thermal Sci. 43 (7) (2004) 689–695.

[6] M. Saadatfar, C.H. Arns, M.A. Knackstedt, T. Senden, Mechanical and transport properties of polymeric foams derived from 3D images, Colloids Surf. A Physicochem. Eng. Aspects 263 (1–3) (2004) 284–289.

[7] R. Coquard, M. Loretz, D. Baillis, Conductive heat transfer in metallic/ceramic open-cell foams, Adv. Eng. Mater. 10 (4) (2008).

[8] J. Petrasch, P. Wyssb, A. Steinfeld, Tomography-based Monte Carlo determination of radiative properties of reticulate porous ceramics, J. Quant. Spectrosc. Radiative Transfer 105 (2) (2007) 180–197.

[9] B. Zeghondy, E. Iacona, J. Taine, Determination of the anisotropic radiative properties of a porous material by radiative distribution function identification (RDFI), Int. J. Heat Mass Transfer 49 (2006) 2810–2819.

[10] B. Zeghondy, E. Iacona, J. Taine, Experimental and RDFI calculated radiative properties of a mullite foam, Int. J. Heat Mass Transfer 49 (2006) 3702–3707.

[11] M. Loretz, R. Coquard, D. Baillis, E. Maire, Metallic foams: radiative properties/comparison between different models, J. Quant. Spectrosc. Radiative Transfer 109 (1) (2008) 16–27.

[12] C.Y. Zhao, T.J. Lu, H.P. Hodson, Thermal radiation in ultralight metal foams with open cells, Int. J. Heat Mass Transfer 47 (14–16) (2004) 2927–2939.

[13] C.Y. Zhao, S.A. Tassou, T.J. Lu, Analytical considerations of thermal radiation in cellular metal foams with open cells, Int. J. Heat Mass Transfer 51 (3–4) (2008) 929–940.

[14] T.J. Lu, C. Chen, Thermal transport and fire retardance properties of cellular aluminium alloys, Acta Mater. 47 (5) (1999) 1469–1485.

[15] M. Wang, N. Pan, Modeling and prediction of the effective thermal conductivity of random open-cell porous foams, Int. J. Heat Mass Transfer 51 (5–6) (2008) 1325–1331.

[16] C.Y. Zhao, T.J. Lua, H.P. Hodson, J.D. Jackson b, The temperature dependence of effective thermal conductivity of open-celled steel alloy foams, Mater. Sci. Eng. A 367 (1–2) (2004) 123–131.

[17] S. André, A. Degiovanni, A theoretical study of the transient coupled conduction and radiation heat transfer in glass phonic conductivity measurements by the Flash technique, Int. J. Heat Mass Transfer 38 (18) (1995) 3401–3412.

[18] S. André, A. Degiovanni, A new way of solving transient radiative–conductive heat transfer problems, J. Heat Transfer 120 (1998) 943–955.

[19] O. Hahn, F. Raether, M.C. Arduini-Schuster, J. Fricke, A. Degiovanni, Transient coupled conductive/radiative heat transfer in absorbing emitting and scattering media: application to laser-flash measurements on ceramic materials, Int. J. Heat Mass Transfer 40 (3) (1997) 689–698.

[20] M. Lazard, S. André, D. Maillet, Diffusivity measurement of semi-transparent media: model of the coupled transient heat transfer and experiments on glass silica glass and zinc selenide, Int. J. Heat Mass Transfer 47 (2004) 477–487.

[21] R. Siegel, J.R. Howell, Thermal Radiation Heat Transfer, third ed., Hemisphere Publishing Corp., Washington, DC, 1992.

[22] R. Viskanta, J. Lim, Transient cooling of a cylindrical glass gob, J. Quant. Spectrosc. Radiative Transfer 73 (2–5) (2002) 3279–3290.

[23] B.G. Carlson, K.D. Lathrop, Transport theory – the method of discrete ordinates, in: H. Greenspan, C.N. Kelber, D. Okrent (Eds.), Computing Methods in Reactor Physics, Gordon and Breach, New-York, 1968, pp. 165–266.

[24] S. Jendoubi, H.S. Lee, T.-K. Kim, Discrete ordinates solution for radiatively participating media in a cylindrical enclosure, J. Thermophys. Heat Transfer 7 (2) (1993) 213–219.

[25] B. Hay, S. Barré, J-R. Filtz, M. Jurion, D. Rochais, P. Sollet, A new apparatus for measuring thermal diffusivity and specific heat of solid at very high temperature, Int. J. Thermophys. 27 (6) (2006) 1803–1815.

[26] S. Gauthier, Contribution à l'étude de la combustion de mélanges gaz naturel-hydrogène en milieu poreux catalytique", Ph.D. thesis, Institut National des Sciences Appliquées (INSA) de Lyon, Villeurbanne, France, 2008.

[27] David R. Clarke, Materials selection guidelines for low thermal conductivity thermal barrier coatings, Surf. Coatings Technol. 163–164 (2003) 67–74.

[28] Michael R. Winter, David R. Clarke, Thermal conductivity of yttria-stabilized zirconia–hafnia solid solutions, Acta Mater. 54 (2006) 5051–5059.

[29] G. Antou, F. Hlawka, A. Cornet, C. Becker, D. Ruch, A. Riche, In situ laser remelted thermal barrier coatings: thermophysical properties, Surf. Coatings Technol. 200 (2006) 6062–6072.

[30] B. Leclercq, R. Mévrel, V. Liedtke, W. Hohenauer, Thermal conductivity of zirconia-based ceramics for thermal barrier coatings, Mat. Wiss. Werkstofftech 34 (2003) 406–409.

[31] R. Barea, M.I. Osendi, J.M.F. Ferreira, P. Miranzo, Thermal conductivity of highly porous mullite material, Acta Mater. 53 (2005) 3313–3318.